Superior Therapeutic Index of Calmangafodipir in Comparison to Mangafodipir as a Chemotherapy Adjunct[1]

Jan Olof G. Karlsson*,†, Tino Kurz*, Susanne Flechsig‡, Jacques Nässström† and Rolf G.G. Andersson*

*Divison of Drug Research/Pharmacology, Department of Medicine and Health Sciences, Linköping University, Linköping, Sweden; †PledPharma AB, Stockholm, Sweden; ‡Experimental Pharmacology and Oncology Berlin-Buch GmbH, Berlin-Buch, Germany

Abstract

Mangafodipir is a magnetic resonance imaging contrast agent with manganese superoxide dismutase (MnSOD) mimetic activity. The MnSOD mimetic activity protects healthy cells against oxidative stress–induced detrimental effects, e.g., myelosuppressive effects of chemotherapy drugs. The contrast property depends on *in vivo* dissociation of Mn^{2+} from mangafodipir—about 80% dissociates after injection. The SOD mimetic activity, however, depends on the intact Mn complex. Complexed Mn^{2+} is readily excreted in the urine, whereas dissociated Mn^{2+} is excreted slowly via the biliary route. Mn is an essential but also a potentially neurotoxic metal. For more frequent therapeutic use, neurotoxicity due to Mn accumulation in the brain may represent a serious problem. Replacement of 4/5 of Mn^{2+} in mangafodipir with Ca^{2+} (resulting in calmangafodipir) stabilizes it from releasing Mn^{2+} after administration, which roughly doubles renal excretion of Mn. A considerable part of Mn^{2+} release from mangafodipir is governed by the presence of a limited amount of plasma zinc (Zn^{2+}). Zn^{2+} has roughly 10^3 and 10^9 times higher affinity than Mn^{2+} and Ca^{2+}, respectively, for fodipir. Replacement of 80% of Mn^{2+} with Ca^{2+} is enough for binding a considerable amount of the readily available plasma Zn^{2+}, resulting in considerably less Mn^{2+} release and retention in the brain and other organs. At equivalent Mn^{2+} doses, calmangafodipir was significantly more efficacious than mangafodipir to protect BALB/c mice against myelosuppressive effects of the chemotherapy drug oxaliplatin. Calmangafodipir did not interfere negatively with the antitumor activity of oxaliplatin in CT26 tumor–bearing syngenic BALB/c mice, contrary calmangafodipir increased the antitumor activity.

Translational Oncology (2012) 5, 492–502

Introduction

Reactive oxygen species (ROS) are known to participate in pathological tissue damage, for instance, during treatment with chemotherapy drugs in cancer patients [1]. The mitochondrial manganese superoxide dismutase (MnSOD) plays a key role in the cellular defense against reactive oxygen–derived free radicals by dismutating superoxide anions ($\cdot O_2^-$), which normally leak from the respiratory chain during mitochondrial reduction of O_2 to H_2O at fairly high amounts. Superoxide is also produced by nicotinamide adenine denucleotide phosphate (NADPH) oxidase. Under normal circumstances, it represents an important mechanism by which neutrophils (NEU) kill invading bacteria and fungi. However, $\cdot O_2^-$ is involved in many pathological conditions, e.g., myocardial ischemia-reperfusion damage, doxorubicin myocardial toxicity, atherosclerosis, and paracetamol hepatotoxicity.

Yet as recently as 45 years ago, oxygen-derived radicals were not thought to occur in living cells. Radicals were thought to be so reactive and unselective that they could not occur in biologic systems. That view changed dramatically in 1967 when Irwin Fridovich and Joe McCord discovered the antioxidant enzyme SOD, a discovery that without doubts belongs to one of the most important biologic discoveries during the last century. Mitochondrial MnSOD catalyzes dismutation of $\cdot O_2^-$ at an extremely high rate ($>10^9$ M^{-1} s^{-1}). The reaction rate is actually close to the diffusion limit of $\cdot O_2^-$ [2], which indicates the immense importance of MnSOD in the cellular defense against oxidative stress. During pathological oxidative stress, the production of $\cdot O_2^-$ exceeds the endogenous protective potential. Moreover, $\cdot O_2^-$ reacts readily with nitric oxide (NO·) to form highly toxic peroxynitrite ($ONOO^-$), which nitrates tyrosine residues of the MnSOD enzyme and irreversibly inactivates the enzyme. Many years ago, this mechanism was suggested to participate in chronic rejection of human renal allografts [3] and recent results indicate nitration of MnSOD to be an early step in paracetamol (acetaminophen)–induced liver failure [4].

The balance between the mitochondrial antioxidant detoxification system and ROS is finely maintained and low levels of mitochondrial ROS are required by cells to modulate normal redox biology [5]. Excessive amounts of ROS, however, are believed to shorten life span and to induce age-associated pathological conditions, such as carcinogenesis, cardiovascular, and other diseases [6].

Although inflammatory processes secondary to oxidative stress damage normal tissue, they may be beneficial to tumor tissue by creating growth factor–rich microenvironment and giving the cancerous clones the need to start growing [7,8]. A body of evidence suggests that whether MnSOD protects normal tissue it may paradoxically make tumor tissue much more sensitive to radiation-induced [9,10] and chemotherapy-induced [11] damaging effects.

The magnetic resonance imaging (MRI) contrast agent manganese dipyridoxyl diphosphate (mangafodipir; MnDPDP) was approved in 1997 for use as a diagnostic MRI contrast agent in humans. Importantly, mangafodipir has also been shown to protect mice against serious side effects of several chemotherapy drugs (doxorubicin, oxaliplatin, and paclitaxel), without interfering negatively with the anticancer effects of these drugs [12–15]. This includes protection against serious reduction in leukocytes [14]. Mangafodipir (i.e., the ready-to-use MRI contrast agent Teslascan) has been tested in one colon cancer patient going through palliative treatment with a combination of folinate, 5-fluorouracil, and oxaliplatin [16], and a first clinical feasibility study in colon cancer patients going through adjuvant 5-fluorouracil plus oxaliplatin (FOLFOX) showing promising results was recently published [17]. Mangafodipir has also been described to protect mice against acetaminophen-induced liver failure [18,19].

Mn is an essential as well as potentially neurotoxic metal. It has been known for many years that under conditions of chronic exposure to high levels of Mn, a syndrome of extrapyramidal dysfunction similar to Parkinson syndrome frequently occurs, although clinically a different disease entity [20]. When a diagnostic MRI dose of mangafodipir is intravenously (i.v.) injected into humans, more than 80% of the administered Mn is released [21,22]. Release of paramagnetic Mn^{2+} is in fact a prerequisite for the diagnostic MRI properties of mangafodipir [22,23]. However, the therapeutic effects of mangafodipir depend on the intact Mn complex [24,25] because Mn undergoes redox cycling (Mn^{2+}/Mn^{3+}) during the catalytic superoxide dismutating cycle [2].

A considerable part of the release of Mn^{2+} from fodipir (DPDP) is governed by the presence of a limited amount of free or loosely bound zinc (Zn^{2+}) in the plasma [21]. Zn^{2+} has roughly 1000 times higher affinity than Mn^{2+} for fodipir [26], and replacement of Mn^{2+} with more loosely bound Ca^{2+} may hence reduce the amount of Mn^{2+} released after injection. Ca^{2+} has approximately 10^6 times lower affinity than Mn^{2+} for fodipir [27].

The present paper describes how replacement of about 4/5 of the Mn^{2+} within mangafodipir with Ca^{2+} considerably stabilizes it from releasing potentially neurotoxic Mn and simultaneously increases the therapeutic efficacy significantly.

Materials and Methods

Test Substances

Calmangafodipir [$Ca_4Mn(DPDP)_5$; Lot No. 11AK0105B; 98.8% pure], mangafodipir (MnDPDP; Lot No.02090106; >99.9% pure), fodipir (DPDP; Lot No. RDL02090206), and PLED [Lot No. KER-AO-122(2)] were exclusively synthesized for PledPharma by Albany Molecular Research, Inc (Albany, NY). The metabolites MnPLED, ZnDPDP, and ZnPLED were gifts from GE Healthcare (Oslo, Norway). Calfodipir (CaDPDP) was prepared by adding equimolar amount of $CaCl_2$ to a stock solution of fodipir (DPDP). Ready-to-use Teslascan (10 mM containing 6 mM ascorbic acid) was from GE Healthcare. Before injection, the test substances were dissolved in 0.9% NaCl solution to suitable strengths.

Oxaliplatin used in the myelosuppressive studies was from Sanofi-aventis (Eloxatin, 5 mg/ml), and that used in the tumor studies was from Teva (Hälsingborg, Sweden). Before injection, oxaliplatin was diluted in 5% glucose to a suitable strength.

Animals

Male Wistar rats (approximately 250 g) used in the excretion studies were from Taconic (Ry, Denmark), whereas male and female rats used in the studies on Mn distributions in the brain and other selected organs after repeated administration were from Charles River (Sulzfeld, Germany). BALB/c female mice (6–8 weeks) used in the myelosuppressive studies were from Charles River, and BALB/c mice (6–8 weeks) used in the tumor studies were from Taconic. The animal experiments were approved by the Ethical Committees on animal research.

Renal Excretion of Mn and Zn in Rats

In a first series of experiments, 10 male Wistar rats (approximately 250 g) were injected i.v., via one of the tail veins, with either 0, 0.125, 0.250, 0.500, or 0.750 ml of a 10 mM fodipir (DPDP) solution, corresponding to 0, 5, 10, 20, and 30 μmol/kg.

In the second series of experiments, eight male Wistar rats (approximately 250 g) were injected i.v., via one of the tail veins, with 0.25 ml of a 50 mM calmangafodipir solution, containing 10 mM Mn^{2+} and 40 mM Ca^{2+}, or 0.25 ml of 10 mM mangafodipir, containing 10 mM Mn^{2+}, corresponding to an Mn^{2+} dose of 10 μmol/kg in both cases. To obtain basal levels of Mn and Zn in urine, two additional (control) rats received 0.25 ml of saline and were placed in metabolic cages for urine collection over the same period of time.

After injection, the rats were immediately placed in metabolic cages for urine collection over a period of up to 24 hours. The urine samples were then stored at –80°C until Mn and Zn analysis. Before analysis, the samples were thawed and extensively shaken to obtain homogenous samples. A 5 ml of aliquot was taken from each sample

and 5 ml concentrated nitric acid was added. The samples were then resolved in a microwave oven and thereafter diluted with distilled water to a final volume of 50 ml. The Mn and Zn contents of each sample were analyzed by inductively coupled plasma mass spectrometry. Identical samples of calmangafodipir and mangafodipir as those injected in the rats (i.e., 0.250 ml) were withdrawn and injected into test tubes. These samples were treated in an identical manner to that of the urine samples and analyzed for its Mn content.

Organ Retention of Mn after Repeated Administration of Calmangafodipir or Mangafodipir in Rats

Wistar male and female rats were i.v. injected with either 0.9% NaCl, 72.0 μmol/kg mangafodipir (corresponding to 72.0 μmol/kg Mn), or 374.4 μmol/kg calmangafodipir (corresponding to 72.0 μmol/kg Mn) three times a week for 13 weeks (each treatment group consisted of nine males and nine females). Each dose of calmangafodipir corresponded to about 36 times the assumed clinical dose. After the 13-week administration period, the rats were killed and the brains and pancreas were dissected out and approximately 0.5 g of samples were stored frozen until Mn analysis. The Mn content of each sample was analyzed by inductively coupled plasma mass spectrometry.

In Vivo Myeloprotective Effects of Calmangafodipir, Mangafodipir, Teslascan, and MnPLED against Oxaliplatin in BALB/c Mice

In a first series of experiments, three groups each consisting of five female BALB/c mice were treated once intraperitoneally (i.p.) with oxaliplatin at 7.5, 10.0, and 12.5 mg/kg oxaliplatin, respectively.

One day before (baseline) as well as 3 and 6 days after oxaliplatin treatment, 50 μl of EDTA blood samples was taken from the orbital venous plexus with a glass capillary. The blood samples were analyzed using the automated system CELL-DYN Emerald (Abbott Diagnostics, Wiesenbaden, Germany) for the content of white blood cells (WBC), lymphocytes (LYM), NEU, and platelets (PLC). CELL-DYN Emerald is accredited for human blood samples. The used device is, however, especially calibrated for mouse blood samples. The CELL-DYN Emerald mouse data obtained at the present laboratory have repeatedly been compared with data from an accredited external laboratory (device: XT2000I; Sysmex, Norderstedt, Germany). These comparisons have always resulted in strong correlations regarding WBC, LYM, and NEU (data not shown).

From the results (Figure 1), it was concluded that further experiments testing the myeloprotective effects of calmangafodipir, mangafodipir, Teslascan, and MnPLED should be performed at 12.5 mg/kg oxaliplatin and that blood cell sample analyses should be performed the day before and 6 days after oxaliplatin administration in every mouse. Thirty minutes before and 24 hours after oxaliplatin administration, mice received saline, calmangafodipir [6.5 μmol/kg; $Ca_4Mn(DPDP)_5$], mangafodipir (1.3 and 13.0 μmol/kg), Teslascan (13.0 μmol/kg), or MnPLED (2.0 μmol/kg) i.v. (five mice in each group). A control group received vehicle (5% glucose) instead of oxaliplatin and saline instead of test substance.

An additional group of five animals received 6.5 μmol/kg (5 mg/kg) calmangafodipir with a treatment schedule identical to the above described experiments (calmangafodipir 30 minutes before and 24 hours after 12.5 mg/kg oxaliplatin; "double dose"). Another group of five mice received just one calmangafodipir treatment, 6.5 μmol/kg,
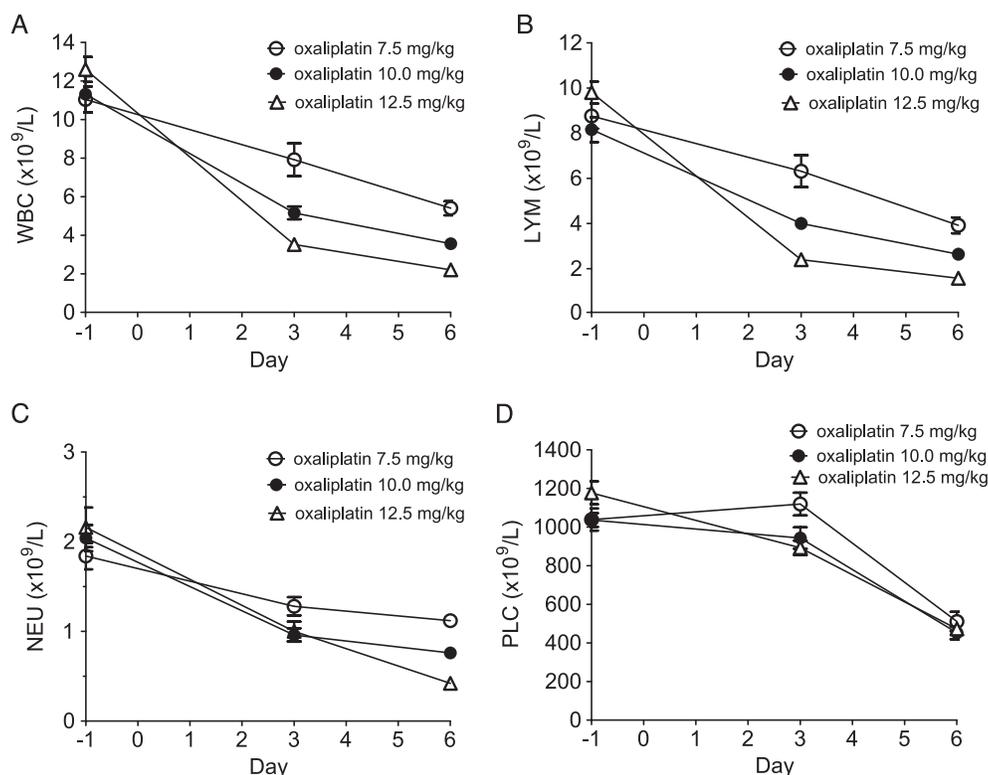

Figure 1. The myelosuppressive effects of increasing single doses (7.5, 10.0, and 12.5 mg/kg) of oxaliplatin on (A) WBC, (B) LYM, (C) NEU, and (D) PLC at 3 and 6 days after injection. Results expressed as mean ± SEM ($n = 5$ in each group).

30 minutes before oxaliplatin ("single dose"). Two further groups of mice receiving either vehicle (i.e., saline plus glucose) or oxaliplatin (i.e., saline plus oxaliplatin) treatment were run in parallel.

The In Vitro Cytotoxic Activity of Calmangafodipir, Mangafodipir, Fodipir, and Metabolites in CT26 Cells

The viability of cells was measured using the methylthiazoletetrazolium assay. Briefly, 8000 CT26 (mouse colon carcinoma) cells were seeded per well on a 96-well plate and grown overnight in Roswell Park Memorial Institute (RPMI) 1640 medium containing 10% FBS, 2 mM L-glutamine, 100 UI/ml penicillin, and 100 μg/ml streptomycin at 37°C in humidified air with 5% CO_2.

In a first series of experiments, cells were exposed to increasing concentrations of oxaliplatin (0.1–100 μM) for 48 hours at 37°C, in the absence and presence of various concentrations of fodipir (10, 30, and 100 μM).

In a second series of experiments, cells were then exposed for 48 hours to 1 to 1000 μM calmangafodipir, fodipir, PLED, calfodipir, mangafodipir, MnPLED, ZnPLED, ZnDPMP, and $CaCl_2$ at 37°C.

The viability of the cells was then assessed by adding 5 mg/ml methylthiazoletetrazolium to a final concentration of 0.5 mg/ml and incubating cells for a further 4 hours at 37°C. The blue formazan that is formed by mitochondrial dehydrogenases of viable cells was then dissolved overnight at 37°C by adding 10% sodium dodecyl sulfate and 10 mM HCl to a final concentration of 5% sodium dodecyl sulfate and 5 mM HCl. Finally, the absorbance of the solution was read at 570 nm with a reference at 670 nm in a microplate reader Spectramax 340 (Molecular Devices, Sunnyvale, CA) connected to an Apple Macintosh computer running the program Softmax Pro V1.2.0 (Molecular Devices).

Antitumor Effects of Oxaliplatin in CT26 Tumor–Bearing Syngenic Mice in the Absence and Presence of Calmangafodipir

CT26 cells were grown in 75-cm² culture flasks in RPMI 1640 medium containing 10% FBS, 2 mM L-glutamine, 100 UI/ml penicillin, and 100 μg/ml streptomycin at 37°C in humidified air with 5% CO_2. When the cells reached ∼50% confluency, they were harvested by trypsinization. Briefly, cells were washed with phosphate-buffered saline (PBS; pH 7.3) and exposed to 0.05% trypsin/0.53 mM EDTA at 37°C for ∼5 minutes. The trypsinization was stopped by adding RPMI 1640 culture medium. Cells were counted and centrifuged at 200*g* for 5 minutes. Thereafter, they were washed in PBS, centrifuged again, and resuspended in PBS at a concentration of 2 × 10⁶/350 μl for injection into mice. Briefly, each mouse was injected subcutaneously in the back of the neck with 2 × 10⁶ of CT26 cells at day 0. After 7 days (day 7) when the tumors were detectable, the tumor size was determined with a caliper and mice were grouped (five in each) so that the sizes of the tumors were not statistically different by group. Oxaliplatin ± calmangafodipir were injected and one group of mice received vehicle (0.9% saline + 5% glucose) treatment alone.

In a first series of experiments, mice were injected i.v. with saline or 50 mg/kg (65 μmol/kg) calmangafodipir 30 minutes before i.p. administration of 20 mg/kg oxaliplatin (diluted in 5% glucose) or 5% glucose. These mice received in addition saline or 65.0 μmol/kg (50 mg/kg) calmangafodipir 24 hours later (day 8). In another series of experiments, mice were injected i.v. with saline or 6.5 μmol/kg (5 mg/kg) or 32.5 μmol/kg (25 mg/kg) calmangafodipir 30 minutes before i.p. administration of 10 mg/kg oxaliplatin (diluted in 5% glucose) or 5% glucose, and saline or 6.5 μmol/kg or 32.5 μmol/kg calmanga-

fodipir 24 hours later (day 8). The mice were killed on day 10 and the tumors were excised, and wet weights (w.w.s) were determined.

Calculations, Presentation of Results, and Statistics

Renal excretion of Mn and Zn are presented as total 0- to 24-hour urine content (expressed as μmol/kg ± SEM) and as percentage (±SEM) of the injected dose. The organ content of Mn is expressed as μg/g w.w. (±SEM). The myelosuppressive effects of oxaliplatin alone and in the presence of calmangafodipir, mangafodipir, Teslascan, or MnPLED are presented in graphs as relative changes from baseline (day –1) for the blood cells (±SEM). The viability of CT26 cells in the presence of an increasing concentration of the various test substances is presented as concentration-response curves (mean ± SD). Where appropriate, the individual curves were fitted to the sigmoidal normalized response logistic equation (Graphpad Prism, version 5.02, La Jolla, CA). From this analysis, the pD_2 (negative log of the concentration of a drug that produces half its maximal response, $-\log EC_{50}$) values of the test substances were calculated; pD_2 values are presented together with 95% confidence intervals. Statistical differences between the other treatments, where appropriate, were tested by Student's *t* test. *P* values lower than .05 were considered as statistically significant differences.

Results

Renal Excretion of Mn and Zn after i.v. Administration of Fodipir, Mangafodipir, and Calmangafodipir

Results from the first series of excretion experiments are shown in Figure 2 (after subtracting basal Zn and Mn excretion). The basal 0- to 24-hour excretion of Zn in two control rats was found to be 0.852 and 0.771 μmol/kg body weight (b.w.), respectively. The 0- to 24-hour Zn excretion more or less saturated around 4 μmol/kg Zn at a dose of 10 μmol/kg fodipir. Fodipir had just minor effects on the Mn excretion. As evident from this figure, fodipir is capable of increasing Zn excretion considerably.

Results from the second series of experiments are shown in Figure 3. Twenty-four hours after i.v. injection of 0.25 ml of 10 mM mangafodipir containing 2.59 μmol Mn, 0.60 ± 0.04 μmol Mn was recovered in urine (Figure 3A), corresponding to 23.1 ± 1.4% of the injected dose (Figure 3B). The corresponding figure after injection of 0.25 ml of 50 mM calmangafodipir containing 2.52 μmol Mn
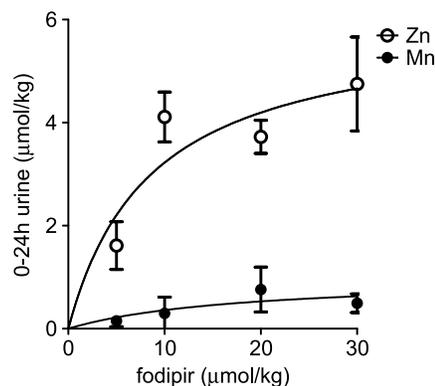

Figure 2. Zero- to twenty-four-hour Zn and Mn renal excretion in rats at increasing doses of fodipir (mean ± SEM; $n = 10$).
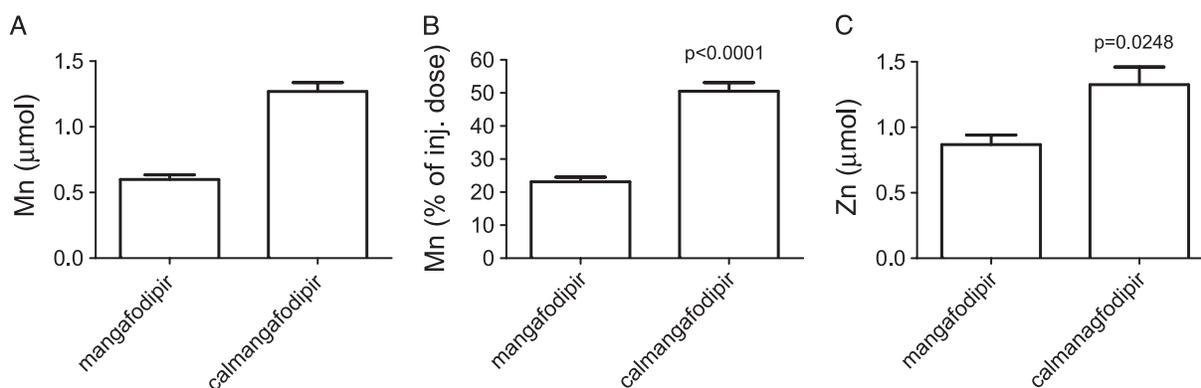
Figure 3. Increase in Mn content in 0- to 24-hour urine from rats injected with mangafodipir or calmangafodipir containing 2.59 μmol and 2.52 μmol Mn, respectively, expressed as (A) the total content of Mn (minus the basal content of Mn) and (B) the percentage of the injected dose. (C) The increase in Zn content in 0- to 24-hour urine in the same animals. Results are expressed as mean ± SEM ($n = 4$ in each group).

was 1.27 ± 0.07 μmol Mn (Figure 3A), corresponding to $50.5 \pm 2.6\%$ of the injected dose (Figure 3B). The difference between mangafodipir and calmangafodipir was highly significant ($P < .0001$). The difference in renal Mn excretion was more or less reflected in the difference in renal excretion of Zn, expressed as increased Zn excretion, i.e., after the basal 24-hour excretion values (0.068 μmol) was subtracted (Figure 3C).

The present results demonstrate how replacement of about 4/5 of the Mn^{2+} in mangafodipir with Ca^{2+}, resulting in calmangafodipir, stabilizes it from releasing Mn^{2+} after i.v. administration, which in turn roughly doubles the amount of Mn^{2+} excreted in the urine.

Organ Retention of Mn after Repeated Administration of Calmangafodipir or Mangafodipir

Results are shown in Figure 4. The Mn brain contents in NaCl-treated control, mangafodipir-treated, and calmangafodipir-treated rats were 0.38 ± 0.01, 0.99 ± 0.02, and 0.74 ± 0.01 μg/g w.w., respectively (Figure 4A), whereas the corresponding Mn contents in the pancreas were 1.66 ± 0.06, 5.54 ± 0.45, and 3.35 ± 0.19 μmol/kg, respectively

(Figure 4B). The levels in control animals were more or less identical to those previously reported in rats by Ni et al. [28]. They reported that the brain and pancreas in control animals contained 6.7 and 26.7 nmol/g w.w., corresponding to 0.37 and 1.5 μg/g w.w., respectively. Although the Mn content of the liver was statistically significantly elevated in the mangafodipir group (Figure 4C), the relative elevation was much less than those seen in the brain and pancreas. A single diagnostic dose of mangafodipir (5 μmol/kg b.w.) is known to cause rapid increase in the Mn content of both the pancreas and the liver of rats—after 2 hours, the Mn content of the pancreas was approximately 10 times higher than the basal value, and the corresponding value of liver was increased about 2 times [28]. Whereas Ni et al. [28] found the Mn content still elevated after 24 hours in the pancreas (about five times the basal value), it was back to baseline in the liver at that time point. This presumably reflects the high capacity of the liver to handle Mn and its important physiological role in Mn homeostasis. This is further supported by the present results showing just a modest increase in liver Mn after heavy exposure to mangafodipir.

As obvious from Figure 4, A and B, calmangafodipir resulted in significantly less retention of Mn compared to mangafodipir, after
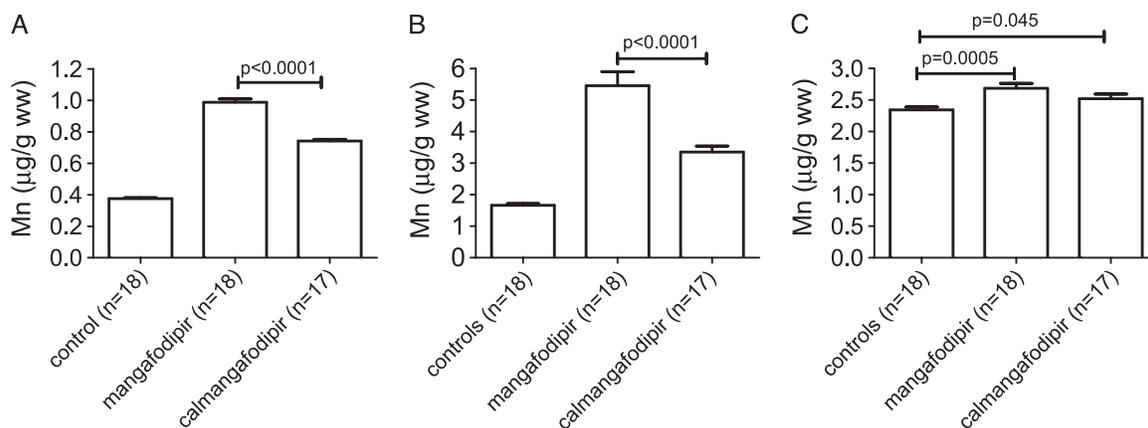

Figure 4. Mn content of the (A) brain, (B) pancreas, and (C) liver, respectively, after 39 doses of either NaCl (controls), mangafodipir, or calmangafodipir (corresponding in both cases to an accumulated dose of 2800 μmol/kg Mn). Results are expressed as mean ± SEM ($n = 17$–18 in each group).

Table 1. Myelosuppressive Effects of a Single Dose of 12.5 mg/kg Oxaliplatin in Untreated BALB/c Mice and in BALB/c Treated with Calmangafodipir [$Ca_4Mn(DPDP)_5$], Mangafodipir (MnDPDP), Teslascan, or MnPLED (Absolute Counts; Mean ± SEM; n = 5).

	WBC (10^9/l)		LYM (10^9/l)		NEU (10^9/l)		PLC (10^9/l)	
	Day −1	Day 6	Day −1	Day 6	Day −1	Day 6	Day −1	Day 6
Saline; oxaliplatin (12.5 mg/g)	12.6 ± 0.6	2.2 ± 0.2	9.8 ± 0.5	1.6 ± 0.2	2.2 ± 0.2	0.4 ± 0.1	1177 ± 59	473 ± 16
$Ca_4Mn(DPDP)_5$ (6.5 µmol/kg); oxaliplatin (12.5 mg/kg)	10.2 ± 0.8	7.3 ± 0.8	7.4 ± 0.8	5.5 ± 0.4	2.3 ± 0.1	1.5 ± 0.4	1038 ± 29	773 ± 143
MnDPDP (1.3 µmol/kg); oxaliplatin (12.5 mg/kg)	10.2 ± 0.5	4.6 ± 0.5	7.7 ± 0.8	3.6 ± 0.4	2.0 ± 0.1	0.9 ± 0.1	957 ± 21	638 ± 117
MnDPDP (13.0 µmol/kg); oxaliplatin (12.5 mg/kg)	11.2 ± 0.6	5.8 ± 0.6	8.8 ± 0.5	4.6 ± 0.5	2.0 ± 0.1	1.0 ± 0.6	908 ± 18	800 ± 100
Teslascan (13.0 µmol/kg); oxaliplatin (12.5 mg/kg)	11.3 ± 0.7	5.2 ± 0.8	9.0 ± 0.6	5.0 ± 0.6	1.8 ± 0.1	1.0 ± 0.2	972 ± 7	693 ± 64
MnPLED (2.0 µmol/kg); oxaliplatin (12.5 mg/kg)	10.1 ± 1.1	7.8 ± 0.7	7.8 ± 0.9	6.4 ± 0.6	1.8 ± 0.2	1.1 ± 0.2	1093 ± 49	857 ± 104

repeated dosing in rats. The total dose in both cases corresponded to approximately 2800 µmol/kg of Mn (39 × 72 µmol/kg). These results demonstrate the improved toxicological profile of calmangafodipir in comparison to that of mangafodipir.

In Vivo *Myeloprotective Effects of Calmangafodipir, Mangafodipir, Teslascan, and MnPLED against Oxaliplatin*

A clear dose-response relationship between increasing doses of oxaliplatin and myelosuppression was evident (Figure 1). As stated in Materials and Methods section, it was concluded that further experi-

ments testing the myeloprotective effects of calmangafodipir, mangafodipir, Teslascan, and MnPLED should be performed at 12.5 mg/kg oxaliplatin and that blood cell sample analyses should be performed the day before and 6 days after oxaliplatin or vehicle administration in every mice.

The absolute pre-values (day −1) and post-values (day 6) of WBC, LYM, NEU, and PLC are given in Table 1. The results, presented as relative differences in cell counts between day −1 and day 6 in each treatment group, are shown in Figure 5. At an equivalent Mn^{2+} dose, i.e., 6.5 µmol/kg (5 mg/kg), calmangafodipir [$Ca_4Mn(DPDP)_5$] was

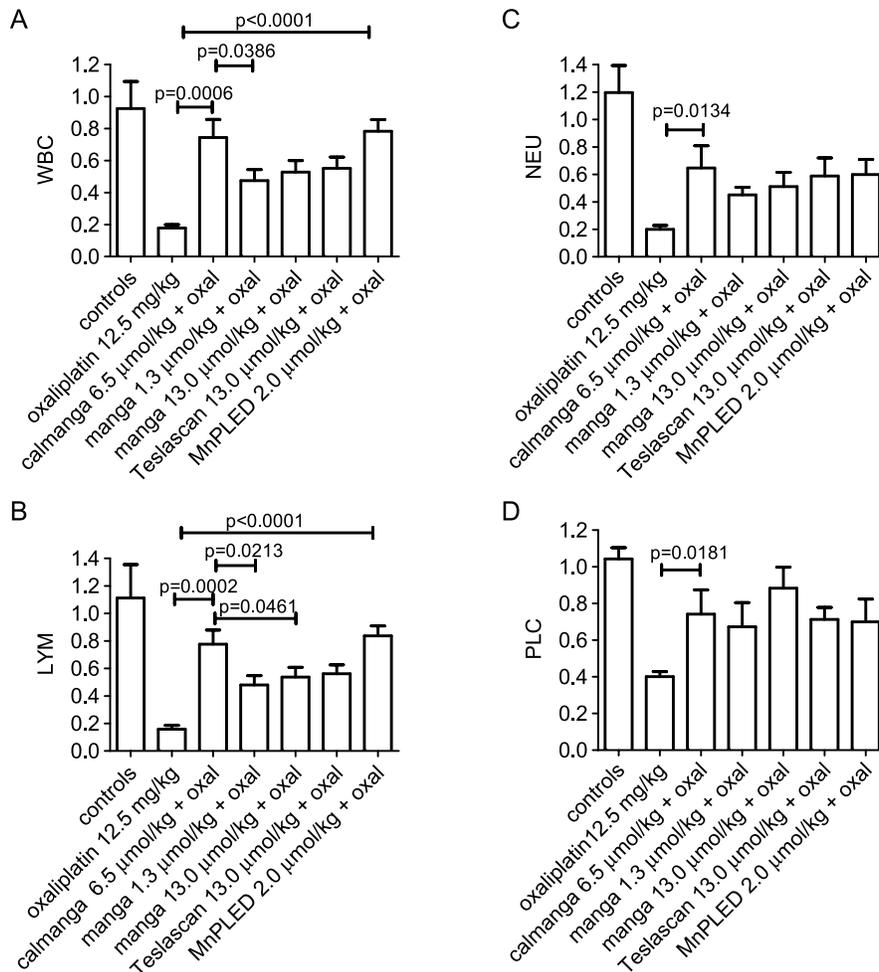**Figure 5.** Myeloprotective effects of calmangafodipir, mangafodipir, Teslascan, and MnPLED with regard to (A) WBC, (B) LYM, (C) NEU, and (D) PLC after oxaliplatin treatment in BALB/c mice. The results are presented as relative differences in cell counts between day −1 and day 6 in each treatment group. Controls received vehicle treatment only. Results expressed as mean ± SEM (n = 5 in each group).

statistically significantly more efficacious than 1.3 µmol/kg (1 mg/kg) mangafodipir (MnDPDP) to protect the mice from oxaliplatin-induced fall in total number of WBC (Figure 5A). A single dose of 12.5 mg/kg oxaliplatin caused the WBC to fall more than 80%, whereas the fall in animals treated with calmangafodipir was only about 25%. The corresponding fall in mice treated with 1.3 or 13.0 µmol/kg mangafodipir was around 50%. Teslascan (13.0 µmol/kg, containing approximately 8 µmol/kg ascorbic acid) gave almost identical results as those of 13.0 µmol/kg mangafodipir, suggesting that ascorbic acid at this particular dose does not influence the protective activity of mangafodipir. Furthermore, the present results presumably also suggest that mangafodipir has to be dephosphorylated into MnPLED before it can exert myeloprotective effects—2 µmol/kg MnPLED was, like cal-mangafodipir, significantly more efficacious than 1.3 and 13.0 µmol/kg mangafodipir to protect WBC. Similar falls were seen in LYM (Figure 5B) and in NEU (Figure 5C) after oxaliplatin treatment, and the test substances gave qualitatively similar protection. Regarding PLC, in comparison to WBC, LYM, and NEU, they differed both in the sensitivity toward oxaliplatin (Figure 1D) and in the cytoprotective effects of the test substances (Figure 5D).

In the above-described studies, the test substances were administered 30 minutes before oxaliplatin and 24 hours after ("double dose"). However, additional experiments comparing the myeloprotective effect of 6.5 µmol/kg calmangafodipir given either as double dose (30 minutes before oxaliplatin and 24 hours after) or as a single dose (30 minutes before oxaliplatin) did not reveal any difference in myeloprotective efficacy (data not shown).

Cytotoxic Activity of Calmangafodipir, Mangafodipir, Fodipir, Calfodipir, and Metabolites in CT26 Cells

Oxaliplatin killed the CT26 cells in a concentration-dependent manner (Figure 6). Neither 10, 30, nor 100 µM fodipir interfered negatively with the cancer cell killing ability of oxaliplatin. An additive effect of 10 µM fodipir was seen in the lower concentration range of oxaliplatin.

When comparing the half-maximal inhibitory concentration (IC_{50}) ratio between calmangafodipir and mangafodipir, the cytotoxic activity of fodipir, PLED, calfodipir, or calmangafodipir was about 20 times higher than that of mangafodipir (Figure 7, A and B; Table 2). MnPLED was six times more potent than mangafodipir (MnDPDP) in its ability to kill CT26 cancer cells. Neither ZnDPDP, ZnPLED, nor $CaCl_2$ displayed any cytotoxic activity. Dissociation of Mn^{2+} from DPDP probably explains, to some extent, the cancer killing efficacy of mangafodipir. Calmangafodipir is, however, almost as efficacious
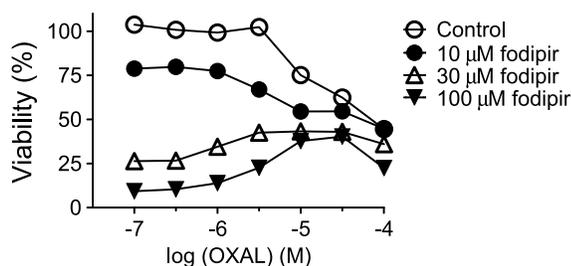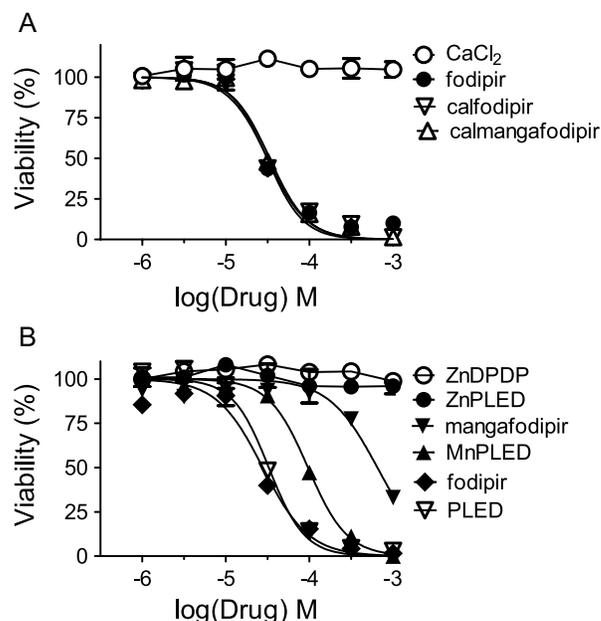

Figure 7. Cytotoxic effects of increasing concentrations of (A) $CaCl_2$, fodipir, calfodipir, and calmangafodipir and (B) ZnDPDP, ZnPLED, mangafodipir, MnPLED, fodipir, and PLED in CT26 cells (mean ± SD; $n = 3$).

as fodipir/calfodipir alone, i.e., the killing efficacy of calmangafodipir is much higher than that of mangafodipir.

The results suggest two important properties. First, PLED is probably as efficacious as its phosphorylated counterpart fodipir (DPDP) with respect to its cancer cell killing ability, and second, the lower *in vitro* stability of MnPLED in comparison to that of MnDPDP [26] probably explains the higher efficacy of MnPLED. The lack of any cytotoxic activity of ZnDPDP and ZnPLED is due to the 1000 times higher stability of these complexes in comparison to their Mn^{2+} counterparts [26].

Antitumor Effects of Oxaliplatin in CT26 Tumor–Bearing Syngenic Mice in the Absence and Presence of Calmangafodipir

In the works on CT26 tumors by Laurent et al. and Alexandre et al. [12,14] conducted in France, they used a model where they allowed the tumor to grow to a size exceeding 10 cm^3. However, to ensure accordance with the European Animal Welfare Guideline 2010/63/EU Article 15 and published guidelines, subcutaneous tumors in mice should not exceed 10% of the animal's own b.w. Therefore, similar to recommendations of Workman et al., studies presented here were finished when tumor volumes exceeded 1.2 cm^3 [29]. Since the CT26 is a fast growing tumor cell line, we had to stop the study 10 days after inoculation of CT26 cells because several of the tumors at that time had reached a size of 1 cm^3. Such a restriction of course makes it more difficult to study treatment-related effects on tumor growth. Nevertheless, we have been able to show a significant difference between oxaliplatin and non–oxaliplatin-treated CT26 tumor–bearing syngenic BALB/c mice.

The results are shown in Figures 8 and 9. In the first series of experiments, the mice received 20 mg/kg oxaliplatin, which is close to the highest tolerated dose. Single treatment with oxaliplatin resulted in a statistically significant and more than 50% reduction in tumor

Figure 6. Cytotoxic effects of oxaliplatin in the absence and presence of various concentrations of DPDP (mean ± SD; $n = 3$).

Table 2. IC$_{50}$, Relative Efficacy (Compared to Fodipir), and pD$_2$ Values of the Test Compounds.

Compound	IC$_{50}$ (M)	Relative Efficacy IC$_{50}$ (Fodipir)/IC$_{50}$ (x^*)	pD$_2$ (95% Confident Limit)†
Fodipir	3.123×10^{-5}	1.0	4.505 (4.432–4.579)
PLED	3.269×10^{-5}	1.0	4.486 (4.439–4.532)
Calmangafodipir	3.351×10^{-5}	0.9	4.475 (4.421–4.529)
Calfodipir	3.153×10^{-5}	1.0	4.501 (4.436–4.567)
Mangafodipir	6.503×10^{-4}	0.05	3.187 (3.103–3.271)
MnPLED	9.628×10^{-5}	0.3	4.016 (3.984–4.048)

*Test compound in question.
†pD$_2$ = −log(IC$_{50}$).

weight. Treatment with calmangafodipir (65.0 µmol/kg) did not have any negative impact on the antitumor effect of oxaliplatin at a high dose (Figure 8). However, in a second series of experiments in which 10 mg/kg oxaliplatin was used, treatment with a relatively low dose of calmangafodipir (6.5 µmol/kg) resulted in a statistically significant better antitumor effect (Figure 9); the combined effect of 10 mg/kg oxaliplatin plus 6.5 µmol/kg calmangafodipir was almost as efficacious as 20 mg/kg oxaliplatin alone. Similar effects were seen after treatment with 32.5 µmol/kg calmangafodipir.

Discussion

When a relevant diagnostic imaging dose of mangafodipir, i.e., 5 to 10 µmol/kg, is injected into humans [21,22], or as in the present study into rats, about 80% of the administered Mn^{2+} is released. For diagnostic imaging purpose and for occasional therapeutic use, dissociation of Mn^{2+} from mangafodipir represents no major toxicological problem. However, for more frequent use, as in therapeutic use, accumulated Mn toxicity may represent a problem, particularly when it comes to neurotoxicity [20,30]. Thus, for frequent therapeutic use, as in cancer treatment, compounds that release Mn should be used with caution.

It is concluded from the present study that replacement of 4/5 of the Mn^{2+} with Ca^{2+} more than doubles the *in vivo* stability of the Mn complex. As obvious from the Results section and Figure 4A, calmangafodipir resulted in significantly and about 40% less retention

of Mn in the brain compared to mangafodipir, after repeated dosing at more than 30 times the assumed clinical dose in rats. The total dose in both cases corresponded to approximately 2800 µmol/kg Mn^{2+} (39 × 72 µmol/kg). These results demonstrate the improved toxicological profile of calmangafodipir in comparison to that of mangafodipir. Furthermore, at equivalent Mn^{2+} doses, calmangafodipir was significantly more efficacious than mangafodipir to protect BALB/c mice against myelosuppressive effects of the chemotherapy drug oxaliplatin. Importantly, calmangafodipir did not interfere negatively with the antitumor effect of oxaliplatin in CT26 tumor–bearing syngenic BALB/c mice. On the contrary, it increased the antitumor effect of oxaliplatin, in a similar way that has been shown with Teslascan (see below) [12]. The improved *in vivo* Mn^{2+} stability of calmangafodipir hence increases its therapeutic index considerably, in comparison to mangafodipir. MnPLED (2 µmol/kg) was, like calmangafodipir, significantly more efficacious than 1.3 and 13.0 µmol/kg mangafodipir to protect WBC, which inevitably suggests that mangafodipir must be dephosphorylated into MnPLED before it can exert *in vivo* myeloprotective effects, in a similar manner that has previously been demonstrated for its cardioprotective effects [15,25].

From the present data, one cannot fully exclude that the higher content of fodipir in calmangafodipir compared to mangafodipir (at an equivalent Mn dose) may have contributed to its higher efficacy. However, the finding that 13 µmol/kg mangafodipir was less efficacious than 6.5 µmol/kg calmangafodipir does not support such a suggestion. Furthermore, a recently published study [15] on myocardial protection of mangafodipir and its metabolite MnPLED
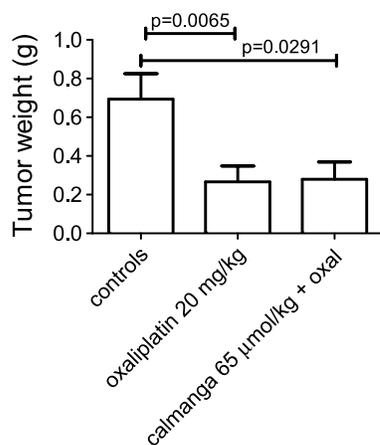
Figure 8. Antitumor effect of a high dose of oxaliplatin (20 mg/kg) in CT26 tumor–bearing syngenic BALB/c mice in the absence and presence of a relatively high dose of calmangafodipir (65.0 µmol/kg). Results expressed as mean ± SEM [n = 10 in vehicle and oxaliplatin (20 mg/kg) groups; n = 5 in the calmangafodipir group].

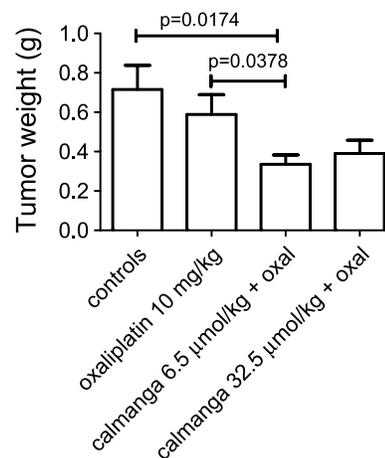**Figure 9.** Antitumor effect of a low dose of oxaliplatin (10 mg/kg) in the absence and presence of 6.5 and 32.5 µmol/kg calmangafodipir. Results are expressed as mean ± SEM (n = 5).

against detrimental effects of doxorubicin (Adriamycin) does not indicate any major effect of fodipir or its metabolite PLED. Studies on the cardioprotective effects of mangafodipir and MnPLED in the pig [25] inevitably show that the protective effect is an inherent property of the intact metal complex and not of either dissociated Mn^{2+} or fodipir/PLED.

In an ideal world, replacement of 4/5 of the Mn^{2+} with Ca^{2+} should cause all administered Mn^{2+} to be excreted in the urine. However, the processes governing the *in vivo* stability of a metal complex like mangafodipir are indeed complicated and hence difficult to predict exactly. Although readily available Zn^{2+} is a main player in the dissociation process of Mn^{2+} from fodipir, other metals present in much higher endogenous concentrations, like Mg^{2+} and Ca^{2+}, will also influence the *in vivo* stability of mangafodipir [27]. Furthermore, the stability constants with regard to these metals differ between mangafodipir and its dephosphorylated metabolite MnPLED [26]. Nevertheless, the *in vivo* stability of Mn^{2+} in calmangafodipir is double that of Mn^{2+} in mangafodipir when tested at an Mn^{2+} dose of 10 µmol/kg, as shown in Figure 3. However, at a more clinically relevant therapeutic dose of Mn^{2+}, i.e., 1 to 2 µmol/kg [17], corresponding to 5 and 10 µmol/kg of calmangafodipir, the relative increase in Mn^{2+} stability will probably be more pronounced. This presumably explains why calmangafodipir at an equivalent dose of Mn^{2+} has an efficacy more than double that of mangafodipir, as evident from Figure 5.

Zn^{2+} is present in all body tissues and fluids. The total body Zn^{2+} content in humans has been estimated to be 2 to 3 g [31]. Plasma Zn^{2+} represents about 0.1% of total body Zn^{2+} content [32], and it is mainly this small fraction of Zn^{2+} that competes with Mn^{2+} for binding to fodipir or its dephosphorylated counterparts, DPMP and PLED, after administration. The human body has a high capacity to maintain Zn homeostasis through synergistic adjustments in gastrointestinal absorption and excretion [31]. Clinical phase 1 studies in humans [21] clearly demonstrated that plasma levels of Zn^{2+} in humans return to baseline within 24 hours after receiving 5 or 10 µmol/kg mangafodipir, i.e., a dose expected to consume a similar amount of Zn^{2+} as that of 6.5 µmol/kg calmangafodipir. It is therefore no or a very low risk that repeated injection of clinically relevant doses calmangafodipir should induce Zn deficiency in patients going through chemotherapy, in case of FOLFOX chemotherapy every second week.

Myelosuppression, in particular neutropenia, is a common dose-limiting event during cancer treatment with many chemotherapy drugs, including among others oxaliplatin. Alexandre et al. [14] have recently shown that 10 mg/kg mangafodipir (Teslascan; corresponding to 13.0 µmol/kg) via its SOD mimetic activity protects mice against paclitaxel-induced leukopenia. The present study demonstrates that 6.5 µmol/kg calmangafodipir (corresponding to 1.3 µmol/kg Mn^{2+}) is considerably more efficacious than 1.3 and 13.0 µmol/kg mangafodipir (corresponding to 1.3 and 13.0 µmol/kg Mn^{2+}, respectively) to protect against severe oxaliplatin-induced leukopenia. In all their experiments where Laurent et al. and Alexandre et al. [12,14] used mangafodipir, they actually used the ready-to-use contrast formulation, i.e., Teslascan, which, in addition to 10 mM mangafodipir, also contains 6 mM antioxidant ascorbic acid. Unfortunately, they did not include any ascorbic acid controls in any of their experiments. The present study shows that the Teslascan dose they used in the *in vivo* experiments, i.e., 10 mg/kg (corresponding to 13.0 µmol/kg), gave more or less identical results as those obtained in the present study with 13 µmol/kg pure mangafodipir. However, in the same papers, they also

studied effects of such a high concentration as 400 µM Teslascan (containing 240 µM ascorbic acid) in various *in vitro* systems, and without any proper ascorbic acid control, it is of course difficult to draw any clear-cut conclusions from such experiments.

It should be stressed that ascorbic acid is added to the ready-to-use formulation of mangafodipir (Teslascan) to avoid oxidation of Mn^{2+} taking place in the vial during storage. However, after *in vivo* administration of a clinically relevant dose of Teslascan, ascorbic acid will have no influence on Mn oxidation. It should also be mentioned that a freshly made water solution of mangafodipir is stable with respect to Mn^{2+} for days without any addition of ascorbic acid. Importantly, during its dismutating action, Mn catalyzes both a one-electron oxidation and a one-electron reduction and is hence electrically neutral [33]. Accordingly, these reactions typically require no external source of redox equivalents and are thus self-contained components of the antioxidant machinery, and there is consequently *per se* no need of a reducing agent like ascorbic acid.

The previously described myeloprotective effect of Teslascan against paclitaxel showed that decrease of peripheral NEU and LYM is accompanied by a parallel decrease in total bone marrow cells [14], which inevitably suggests that mangafodipir exerts its protective effect at the level of myelopoiesis.

The reason why mangafodipir and calmangafodipir protects non-malignant cells but damages cancer cells is far from well understood. The present paper and a recent paper by Kurz et al. [15] show that the *in vitro* cytotoxic activity of mangafodipir is an inherent property of fodipir or its dephosphorylated counterpart PLED alone and not of the intact Mn^{2+} complex. Speculatively, it may be that cancer cells preferably take up the dissociated form of fodipir or its dephosphorylated counterparts, whereas the intact Mn^{2+} complex is preferably taken up by non-malignant cells, in analogy with that described for the antioxidant amifostine [34]. When it comes to the *in vivo* behavior of mangafodipir, it seems, however, reasonable to look for additional/ alternative explanations. The complicated *in vivo* metabolic pattern of mangafodipir, involving stepwise dephosphorylation and Mn^{2+} release [21], makes it difficult to draw conclusions from *in vitro* experiments.

Some important clues may be obtained from research aiming to find selective radioprotectants. A body of evidence demonstrates that overexpression of MnSOD protects non-malignant tissues against radiation-induced oxidative stress and, interestingly, simultaneously makes cancer cells more susceptible to radiation [9,10].

However, the experimental and clinical use of SOD enzymes has been restricted due to large molecular weight and poor cellular uptake [35]. To circumvent this limitation experimentally, transgenic animal models have been used to study the radioprotective potential of MnSOD enzymes. These studies have demonstrated that treating radiated animal models with MnSOD, delivered by injection of the enzyme through liposome/viral-mediated gene therapy or insertion of the human MnSOD gene, can ameliorate radiation-induced damage [10,36] and simultaneously make cancerous tissue more susceptible to radiation [9].

It is known that reduced MnSOD expression contributes to increased DNA damage, and cancer cell lines often have diminished MnSOD activity compared to normal counterparts [5,37,38]. Mutations within the MnSOD gene and its regulatory sequence have been observed in several types of human cancers [5,38–40]. In addition to cancer, mutations in MnSOD are associated with cardiomyopathy and neuronal diseases, demonstrating the significant role of MnSOD activity in age-related illnesses [6].

An elevated oxidative status is indispensable for mitogenic stimulation in transformed cells [41]. A number of studies have reported that ROS play an important role in promoting tumor metastasis [8,38,42–45]. These data are consistent with a large body of literature suggesting that the redox balance of many epithelial tumor cells favors an elevated oxidant set point [1], including CT26 cells [12,14]. MnSOD is suppressing cell growth in a variety of cancer cell lines and in mouse models, and the MnSOD growth–retarding functions are at least partially due to triggering of a p53-dependent cellular senescence program [46]. Transfection of human MnSOD cDNA into MCF-7 human breast cancer cells, UACC-903 human melanoma cells, SCC-25 human oral squamous carcinoma cells, U118 human glioma cells, and DU145 human prostate carcinoma cells significantly suppressed their malignant phenotype [40,47–50]. Furthermore, overexpression of MnSOD induced growth arrest in the human colorectal cancer cell line HCT116 and increased senescence that required the induction of p53 [46]. Introduction of the normal MnSOD gene in cancer cells alters the phenotype and the cells lose the ability to form colonies in culture and tumors in nude mice [47].

Although inflammatory processes secondary to oxidative stress damage normal tissue, they may, in fact, be beneficial to tumor tissue by creating growth factor–rich microenvironment and giving the cancerous clones the need to start growing [7,8]. A striking example is the existence of tumor-associated macrophages that accumulate preferentially in the poorly vascularized regions of tumors and secrete cytokines that actually promote tumor growth [8]. Moreover, not only can these cytokines promote tumor growth but they have also been shown to suppress activation of $CD8^+$ T-LYM that are most efficient in tumor elimination. In fact, there is an increasing interest for the importance of T-LYM–mediated immune response for the outcome of cancer chemotherapy [51]. It is known that severe lymphopenia (<1000 cells/µl) negatively affects the chemotherapy response. A collection of mouse cancers, including CT26 colon cancer, MCA205 fibrosarcomas, TSA cell line breast cancers, GOS cell line osteosarcomas, and EL4 thymomas, respond to chemotherapy with doxorubicin and oxaliplatin much more efficiently when they are implanted in syngenic immune-competent mice than in immune-deficient hosts, i.e., nude mice [51]. This is in line with clinical studies revealing that interferon-gamma (IFN-γ)–producing $CD8^+$ T-LYM are potent cancer immune effectors. Furthermore, a high NEU/LYM ratio is associated with a low overall survival for patients with advanced colorectal cancer [52]. Taking into consideration that mangafodipir and in particular calmangafodipir are highly efficient LYM-protecting agents during chemotherapy, it is plausible that this property is of particular importance during *in vivo* conditions.

From the above discussion, MnSOD appears as an ideal target for adjunct/supportive treatment in connection with chemotherapy and radiotherapy—by simultaneously making cancer cells more susceptible to chemotherapy and radiotherapy and by protecting normal tissue against oxidative damage. Although gene therapy theoretically may offer a therapeutic possibility, cell permeable low molecular weight MnSOD mimetics represent a superior alternative. Kensler et al. described the anticarcinogenic activity of the first generation of a copper superoxide dismutase (CuSOD) mimetic already in 1983 [53]. They were followed by MnSOD mimetics, particularly of the so-called metalloporphyrin, salen, and macrocyclic types, and most recently by the so-called MnPLED derivatives [24,54,55]. A few of the MnSOD mimetics, including the MnPLED derivative mangafodipir, have been tested in patients. In a small phase II translational study,

mangafodipir was shown to protect against dose-limiting toxicity of chemotherapy in cancer patients [17].

Taken together, the present study shows a superior therapeutic efficacy of calmangafodipir in comparison to mangafodipir, with respect to selective protection against chemotherapy-induced tissue damage.

References

[1] Doroshow JH (2006). Redox modulation of chemotherapy-induced tumor cell killing and normal tissue toxicity [editorial]. *J Natl Cancer Inst* **98**, 223–225.

[2] Fridovich I (1998). Oxygen toxicity: a radical explanation. *J Exp Biol* **201**, 1203–1209.

[3] MacMillan-Crow LA, Crow JP, Kerby JD, Beckman JS, and Thompson JA (1996). Nitration and inactivation of manganese superoxide dismutase in chronic rejection of human renal allografts. *Proc Natl Acad Sci USA* **93**, 11853–11858.

[4] Agarwal R, Macmillan-Crow LA, Rafferty TM, Saba H, Roberts DW, Fifer EK, James LP, and Hinson JA (2010). Acetaminophen-induced hepatotoxicity in mice occurs with inhibition of activity and nitration of mitochondrial manganese superoxide dismutase. *J Pharmacol Exp Ther* **337**, 110–118.

[5] Buettner GR (2011). Superoxide dismutase in redox biology: the roles of superoxide and hydrogen peroxide. *Anticancer Agents Med Chem* **11**, 341–346.

[6] Ozden O, Park SH, Kim HS, Jiang H, Coleman MC, Spitz DR, and Gius D (2011). Acetylation of MnSOD directs enzymatic activity responding to cellular nutrient status or oxidative stress. *Aging (Albany NY)* **3**, 102–107.

[7] Anscher MS (2010). Targeting the TGF-β₁ pathway to prevent normal tissue injury after cancer therapy. *Oncologist* **15**, 350–359.

[8] Kareva I (2011). What can ecology teach us about cancer? *Transl Oncol* **4**, 266–270.

[9] Urano M, Kuroda M, Reynolds R, Oberley TD, and St Clair DK (1995). Expression of manganese superoxide dismutase reduces tumor control radiation dose: gene-radiotherapy. *Cancer Res* **55**, 2490–2493.

[10] Borrelli A, Schiattarella A, Mancini R, Morrica B, Cerciello V, Mormile M, d'Alesio V, Bottalico L, Morelli F, D'Armiento M, et al. (2009). A recombinant MnSOD is radioprotective for normal cells and radiosensitizing for tumor cells. *Free Radic Biol Med* **46**, 110–116.

[11] Oberley LW (2001). Anticancer therapy by overexpression of superoxide dismutase. *Antioxid Redox Signal* **3**, 461–472.

[12] Laurent A, Nicco C, Chéreau C, Goulvestre C, Alexandre J, Alves A, Lévy E, Goldwasser F, Panis Y, Soubrane O, et al. (2005). Controlling tumor growth by modulating endogenous production of reactive oxygen species. *Cancer Res* **65**, 948–956.

[13] Karlsson JOG, Brurok H, Towart R, and Jynge P (2006). The magnetic resonance imaging contrast agent mangafodipir exerts antitumor activity via a previously described superoxide dismutase mimetic activity [letter to the editor]. *Cancer Res* **66**, 598.

[14] Alexandre J, Nicco C, Chéreau C, Laurent A, Weill B, Goldwasser F, and Batteux F (2006). Improvement of the therapeutic index of anticancer drugs by the superoxide dismutase mimic mangafodipir. *J Natl Cancer Inst* **98**, 236–244.

[15] Kurz T, Grant D, Andersson RGG, Towart R, De Cesare M, and Karlsson JOG (2012). Effects of MnDPDP and ICRF-187 on doxorubicin-induced cardiotoxicity and anticancer activity. *Transl Oncol* **5**, 252–259.

[16] Yri OE, Vig J, Hegstad E, Hovde O, Pignon I, and Jynge P (2009). Mangafodipir as a cytoprotective adjunct to chemotherapy—a case report. *Acta Oncol* **48**, 633–635.

[17] Karlsson JO, Adolfsson K, Thelin B, Jynge P, Andersson RG, and Falkmer UG (2012). First clinical experience with the magnetic resonance imaging contrast agent and superoxide dismutase mimetic mangafodipir as an adjunct in cancer chemotherapy—a translational study. *Transl Oncol* **5**, 32–38.

[18] Bedda S, Laurent A, Conti F, Chéreau C, Tran A, Tran-Van Nhieu J, Jaffray P, Soubrane O, Goulvestre C, Calmus Y, et al. (2003). Mangafodipir prevents liver injury induced by acetaminophen in the mouse. *J Hepatol* **39**, 765–772.

[19] Karlsson JOG (2004). Antioxidant activity of mangafodipir is not a new finding [letter to the editor]. *J Hepatol* **40**, 872–873.

[20] Scheuhammer AM and Cherian MG (1982). Influence of chronic MnCl₂ and EDTA treatment on tissue levels and urinary excretion of trace metals in rats. *Arch Environ Contam Toxicol* **11**, 515–520.

[21] Toft KG, Hustvedt SO, Grant D, Martinsen I, Gordon PB, Friisk GA, Korsmo AJ, and Skotland T (1997). Metabolism and pharmacokinetics of MnDPDP in man. *Acta Radiol* **38**, 677–689.

[22] Southon TE, Grant D, Bjørnerud A, Moen OM, Spilling B, Martinsen I, and Refsum H (1997). NMR relaxation studies with MnDPDP. *Acta Radiol* **38**, 708–716.

[23] Wendland MF (2004). Applications of manganese-enhanced magnetic resonance imaging (MEMRI) to imaging of the heart. *NMR Biomed* **17**, 581–594.

[24] Brurok H, Ardenkjaer-Larsen JH, Hansson G, Skarra S, Berg K, Karlsson JO, Laursen I, and Jynge P (1999). Manganese dipyridoxyl diphosphate: MRI contrast agent with antioxidative and cardioprotective properties? *Biochem Biophys Res Commun* **254**, 768–772.

[25] Karlsson JOG, Brurok H, Eriksen M, Towart R, Toft KG, Moen O, Engebretsen B, Jynge P, and Refsum H (2001). Cardioprotective effects of the MR contrast agent MnDPDP and its metabolite MnPLED upon reperfusion of the ischemic porcine myocardium. *Acta Radiol* **42**, 540–547.

[26] Rocklage SM, Cacheris WP, Quay SC, Hahn FE, and Raymond KN (1989). Manganese(II) N,N'-dipyridoxylethylenediamine-N,N'-diacetate 5,5-bis (phosphate). Synthesis and characterization of a paramagnetic chelate for magnetic resonance imaging enhancement. *Inorg Chem* **28**, 477–485.

[27] Schmidt PP, Toft KG, Skotland T, and Andersson K (2002). Stability and transmetallation of the magnetic resonance contrast agent MnDPDP measured by EPR. *J Biol Inorg Chem* **7**, 241–248.

[28] Ni Y, Petré C, Bosmans H, Miao Y, Grant D, Baert AL, and Marchal G (1997). Comparison of manganese biodistribution and MR contrast enhancement in rats after intravenous injection of MnDPDP and $MnCl_2$. *Acta Radiol* **38**, 700–707.

[29] Workman P, Aboagye EO, Balkwill F, Balmain A, Bruder G, Chaplin DJ, Double JA, Everitt J, Farningham DA, Glennie MJ, et al. (2010). Guidelines for the welfare and use of animals in cancer research. *Br J Cancer* **102**, 1555–1577.

[30] Crossgrove J and Zheng W (2004). Manganese toxicity upon overexposure. *NMR Biomed* **17**, 544–553.

[31] King JC, Shames DM, and Woodhouse LR (2000). Zinc homeostasis in humans. *J Nutr* **130**, 1360S–1366S.

[32] Folin M, Contiero E, and Vaselli GM (1994). Zinc content of normal human serum and its correlation with some hematic parameters. *Biometals* **7**, 75–79.

[33] Culotta VC, Yang M, and O'Halloran TV (2006). Activation of superoxide dismutases: putting the metal to the pedal. *Biochim Biophys Acta* **1763**, 747–758.

[34] Yuhas JM (1980). Active versus passive absorption kinetics as the basis for selective protection of normal tissues by S-2-(3-aminopropylamino)-ethylphosphorothioic acid. *Cancer Res* **40**, 1519–1524.

[35] Citrin D, Cotrim AP, Hyodo F, Baum BJ, Krishna MC, and Mitchell JB (2010). Radioprotectors and mitigators of radiation-induced normal tissue injury. *Oncologist* **15**, 360–371.

[36] Kang SK, Rabbani ZN, Folz RJ, Golson ML, Huang H, Yu D, Samulski TS, Dewhirst MW, Anscher MS, and Vujaskovic Z (2003). Overexpression of extracellular superoxide dismutase protects mice from radiation-induced lung injury. *Int J Radiat Oncol Biol Phys* **57**, 1056–1066.

[37] Oberley LW and Buettner GR (2003). Role of superoxide dismutase in cancer: a review. *Cancer Res* **39**, 1141–1149.

[38] Li C and Zhou HM (2011). The role of manganese superoxide dismutase in inflammation defense. *Enzyme Res* **2011**, 387176. E-pub 2011 Oct 3.

[39] Xu Y, Fang F, Dhar SK, Bosch A, St Clair WH, Kasarskis EJ, and St Clair DK (2008). Mutations in the *SOD2* promoter reveal a molecular basis for an activating protein 2-dependent dysregulation of manganese superoxide dismutase expression in cancer cells. *Mol Cancer Res* **6**, 1881–1893.

[40] Zhang HJ, Yan T, Oberley TD, and Oberley LW (1999). Comparison of effects of two polymorphic variants of manganese superoxide dismutase on human breast MCF-7 cancer cell phenotype. *Cancer Res* **59**, 6276–6283.

[41] Irani K, Xia Y, Zweier JL, Sollott SJ, Der CJ, Fearon ER, Sundaresan M, Finkel T, and Goldschmidt-Clermont PJ (1997). Mitogenic signaling mediated by oxidants in Ras-transformed fibroblasts. *Science* **275**, 1649–1652.

[42] Cerutti PA (1985). Prooxidant states and tumor promotion. *Science* **227**, 375–381.

[43] Szatrowski TP and Nathan CF (1991). Production of large amounts of hydrogen peroxide by human tumor cells. *Cancer Res* **51**, 794–798.

[44] Benhar M, Dalyot I, Engelberg D, and Levitzki A (2001). Enhanced ROS production in oncogenically transformed cells potentiates c-Jun N-terminal kinase and p38 mitogen-activated protein kinase activation and sensitization to genotoxic stress. *Mol Cell Biol* **21**, 6913–6926.

[45] Cullen JJ, Weydert C, Hinkhouse MM, Ritchie J, Domann FE, Spitz D, and Oberley LW (2003). The role of manganese superoxide dismutase in the growth of pancreatic adenocarcinoma. *Cancer Res* **63**, 1297–1303.

[46] Behrend L, Mohr A, Dick T, and Zwacka RM (2005). Manganese superoxide dismutase induces p53-dependent senescence in colorectal cancer cells. *Mol Cell Biol* **25**, 7758–7769.

[47] Church SL, Grant JW, Ridnour LA, Oberley LW, Swanson PE, Meltzer PS, and Trent JM (1993). Increased manganese superoxide dismutase expression suppresses the malignant phenotype of human melanoma cells. *Proc Natl Acad Sci USA* **90**, 3113–3117.

[48] Zhong W, Oberley LW, Oberley TD, and St Clair DK (1997). Suppression of the malignant phenotype of human glioma cells by overexpression of manganese superoxide dismutase. *Oncogene* **14**, 481–490.

[49] Liu R, Oberley LW, and Oberley TD (1997). Transfection and expression of MnSOD cDNA decreases tumor malignancy of human oral squamous carcinoma SCC-25 cells. *Hum Gene Ther* **8**, 585–595.

[50] Li Y, Huang TT, Carlson EJ, Melov S, Ursell PC, Olson JL, Noble LJ, Yoshimura MP, Li N, Oberley TD, et al. (1998). Overexpression of manganese superoxide dismutase in DU145 human prostate carcinoma cells has multiple effects on cell phenotype. *Prostate* **35**, 221–233.

[51] Zitvogel L, Kepp O, and Kroemer G (2011). Immune parameters affecting the efficacy of chemotherapeutic regimens. *Nat Rev Clin Oncol* **8**, 151–160.

[52] Chua W, Charles KA, Baracos VE, and Clarke SJ (2011). Neutrophil/lymphocyte ratio predicts chemotherapy outcomes in patients with advanced colorectal cancer. *Br J Cancer* **104**, 1288–1295.

[53] Kensler TW, Bush DM, and Kozumbo WJ (1983). Inhibition of tumour promotion by a biomimetic SOD. *Science* **221**, 75–81.

[54] Asplund A, Grant D, and Karlsson JOG (1994). Mangafodipir (MnDPDP)- and $MnCl_2$-induced endothelium-dependent relaxation in bovine mesenteric arteries. *J Pharmacol Exp Ther* **271**, 609–618.

[55] Miriyala S, Spasojevic I, Tovmasyan A, Salvemini D, Vujaskovic Z, St Clair D, and Batinic-Haberle I (2012). Manganese superoxide dismutase, MnSOD and its mimics. *Biochim Biophys Acta* **1822**, 794–814.